Metformin—an Adjunct Antineoplastic Therapy—Divergently Modulates Tumor Metabolism and Proliferation, Interfering with Early Response Prediction by ^{18}F-FDG PET Imaging

Peiman Habibollahi*[1], Nynke S. van den Berg*[1], Darshini Kuruppu[1], Massimo Loda[2], and Umar Mahmood[1]

[1]*Division of Nuclear Medicine and Molecular Imaging, Department of Radiology, Massachusetts General Hospital, Harvard Medical School, Boston, Massachusetts; and* [2]*Department of Pathology, Dana-Farber Cancer Institute, Harvard Medical School, Boston, Massachusetts*

Over the last several years, epidemiologic data have suggested that the antidiabetes drug metformin (MET), an adenosine monophosphate–activated protein kinase (AMPK) activator, improves progression-free survival of patients with multiple cancers; more than 30 clinical trials are under way to confirm this finding. We postulated that the role of AMPK as a central cellular energy sensor would result in opposite effects on glucose uptake and proliferation, suggesting different roles for ^{18}F-FDG and 3′-deoxy-3′-^{18}F-fluorothymidine (^{18}F-FLT) in assessing its effectiveness as an antineoplastic agent. **Methods:** Colon cancer cell lines HT29 (human) and MC26 (murine) were treated for 24 or 72 h with a range of MET concentrations (0–10 mM). Western blotting was used to study the activation of AMPK after MET treatment. Glucose uptake and cell proliferation were measured by cell retention studies with either ^{18}F-FDG or ^{18}F-FLT. EdU (ethynyl deoxyuridine, a thymidine analog) and annexin-propidium iodide flow cytometry was performed to determine cell cycle S-phase and apoptotic changes. In vivo ^{18}F-FDG and ^{18}F-FLT PET images were acquired before and 24 h after MET treatment of HT29 tumor–bearing mice. **Results:** After 24 h of MET incubation, phosphorylated AMPK levels increased severalfold in both cell lines, whereas total AMPK levels remained unchanged. In cell retention studies, ^{18}F-FDG uptake increased but ^{18}F-FLT retention decreased significantly in both cell lines. The numbers of HT29 and MC26 cells in the S phase decreased 36% and 33%, respectively, after MET therapy. Apoptosis increased 10.5-fold and 5.8-fold in HT29 and MC26 cells, respectively, after 72 h of incubation with MET. PET imaging revealed increased ^{18}F-FDG uptake (mean ± SEM standardized uptake values were 0.71 ± 0.03 before and 1.29 ± 0.11 after MET therapy) ($P < 0.05$) and decreased ^{18}F-FLT uptake (mean ± SEM standardized uptake values were 1.18 ± 0.05 before and 0.89 ± 0.01 after MET therapy) ($P < 0.05$) in HT29 tumor–bearing mice. **Conclusion:** MET, through activation of the AMPK pathway, produces a dose-dependent increase in tumor glucose uptake while decreasing cell proliferation in human and murine colon cancer cells. Thus, changes in ^{18}F-FDG uptake after MET treatment may be misleading. ^{18}F-FLT imaging is a promising alternative that correlates with the tumor response.

Key Words: metformin; AMPK; tumor metabolic imaging; proliferation imaging

J Nucl Med 2013; 54:252–258
DOI: 10.2967/jnumed.112.107011

Metformin (MET) is a biguanide drug that has been used for decades for the treatment of diabetes type II. Recently, reduced cancer risks in patients using MET for diabetes were reported in epidemiologic studies (*1,2*). Studies have also confirmed decreased overall and cancer-related mortality in some cancer patients (*3*). As a result of increasing interest in the role of metabolic modulators such as MET in improving progression-free survival in cancer patients, over 30 clinical trials with MET in combination chemotherapy regimens for locally advanced or metastatic cancers are now under way to confirm this finding (*4–6*). These trials encompass a variety of cancers, such as prostate, breast, and colorectal cancer, lymphoma, and leukemia. Preclinical studies have already confirmed delayed tumor onset and tumor growth after MET treatment in mouse models of cancer (*7–10*) as well as an increased tumor response in cancer cell lines when MET was combined with chemotherapy (*11*). Moreover, reduced proliferation (*9*) and colony formation (*9,11,12*), induction of apoptosis (*9,13*), and cell cycle arrest (*9,10,12*) have been demonstrated in various cancer cell lines after MET therapy.

MET directly and indirectly activates adenosine monophosphate–activated protein kinase (AMPK) through the inhibition of mitochondrial respiratory complex I (*14,15*). The cellular energy sensor AMPK is part of the liver kinase B1/AMPK/mammalian target of rapamycin (LKB1/AMPK/mTOR) pathway, controlling cellular metabolism and survival (*16*). Once activated, AMPK inhibits mTORC1 through the activation of tuberous sclerosis complex II, resulting in mTOR inhibition (*16*). AMPK activation results

Received Apr. 2, 2012; revision accepted Aug. 24, 2012.
For correspondence or reprints contact: Umar Mahmood, Division of Nuclear Medicine and Molecular Imaging, Department of Radiology, Massachusetts General Hospital, Harvard Medical School, 55 Fruit St., Boston, MA 02114.
E-mail: umahmood@mgh.harvard.edu
*Contributed equally to this work.

in the inhibition of energy-consuming processes (e.g., DNA proliferation, protein synthesis, and lipid synthesis) and the activation of adenosine triphosphate–producing processes (e.g., glucose uptake from circulation and fatty acid oxidation) (*15,17*). We hypothesized that these alterations in glucose metabolism and proliferative activities of the cells would divergently modulate the uptake of metabolic and proliferative radiotracers, such as ^{18}F-FDG and 3′-deoxy-3′-^{18}F-fluorothymidine (^{18}F-FLT), respectively, that are used to image the functional properties of cancer cells (Fig. 1).

Although MET and other glucose modulators are widely used in patients with diabetes and play increasingly important roles in cancer therapy, little is known about the impact of metabolic modulators of glucose on PET imaging in cancer. Previous reports are limited to descriptions of reversible increased bowel uptake as a result of MET treatment (*18,19*). It has also been reported that glucose modulators such as rosiglitazone, but not MET, may increase overall glucose uptake and blood flow in adipose tissue (*20*). Considering AMPK as the primary target for MET and its role as the main cellular energy sensor, we postulated that MET would result in opposite effects on glucose uptake and cellular proliferation in tumors and thereby would adversely affect the ability of ^{18}F-FDG PET to predict the response to therapy. We further hypothesized that proliferation markers such as ^{18}F-FLT would directly correlate with the antineoplastic effects of MET and enable optimization of the dosing of MET in combination with other antineoplastic regimens. We investigated these effects both in vitro and in vivo after treatment of HT29 (human) and MC26 (murine) colon cancer cell lines with various concentrations of MET for 24 or 72 h.

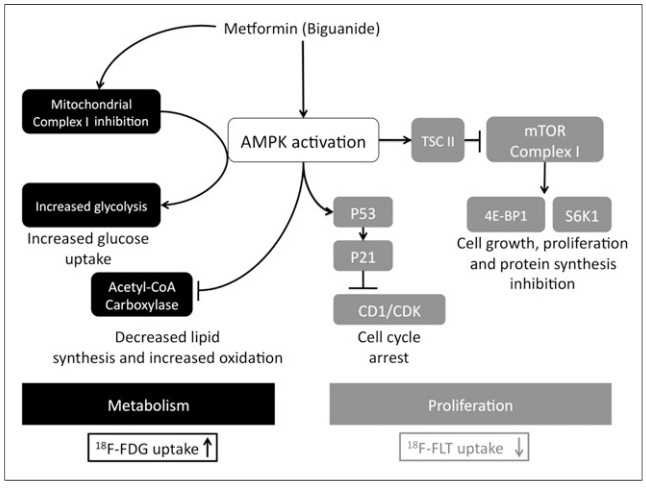

FIGURE 1. MET mechanism of action. MET activates AMPK (main energy sensor in cells), mimicking starvation conditions inside cells. In response to AMPK activation, all energy-consuming pathways are downregulated and adenosine triphosphate–producing mechanisms (such as glycolysis) are increased. CoA = coenzyme A; mTOR = mammalian target of rapamycin; TSC = tuberous sclerosis complex.

MATERIALS AND METHODS

Cell Cultures

Human colon cancer cell line HT29 (American Type Culture Collection) and mouse colon cancer cell line MC26 (American Type Culture Collection) were grown in RPMI medium containing L-glutamine (cellgro by Mediatech) and Dulbecco minimum essential medium containing L-glutamine and sodium pyruvate (cellgro by Mediatech), respectively. The media were supplemented with 10% fetal bovine serum (Atlanta Biologicals) and 1% penicillin–streptomycin (cellgro by Mediatech). The cells were maintained in a humidified incubator at 37°C with 5% CO_2.

Western Blotting

HT29 cells (5×10^5) and MC26 cells (1.5×10^5) were plated in 6-well dishes and allowed to attach overnight. The cells were incubated for 24 h with 0–10 mM MET (Sigma-Aldrich) dissolved in fresh culture medium. After the cells were washed twice in cold phosphate-buffered saline (PBS), 100 μL of lysis buffer (1 tablet of protease inhibitor [Roche] and phosphatase inhibitor cocktails 2 and 3 [both 1:100; Sigma-Aldrich] in 10 mL of NP-40 [Boston Bioproducts]) were added to each well, and the mixtures were incubated for 15 min at 4°C on a plate rocker to completely lyse the cells. After scraping, the cell suspension was transferred to a 1.5-mL Eppendorf tube and centrifuged (15 min; 4°C; 13,000 rpm). The supernatant was collected in a fresh Eppendorf tube and stored at −80°C for further analysis.

The protein concentrations in the lysates were determined with a Pierce bicinchoninic acid protein assay kit (Thermo Scientific). The samples (30 μg of protein) were loaded on 4%–15% TGX precast gels (Bio-Rad) for electrophoresis after dilution with Laemmli sample buffer (1:1; Bio-Rad) and denaturation at 97°C for 5 min. After electrophoresis, the gels were blotted on polyvinylidene difluoride membranes (Roche), and the membranes were blocked with blocking buffer (1% blocking-grade nonfat dry milk; Bio-Rad) in Tris-buffered saline–0.1% polysorbate (Sigma-Aldrich) and incubated with phospho-AMPKα (1:1,000 dilution), AMPKα antibody (1:1,000 dilution), and β-actin antibody (1:3,000 dilution) (all from Cell Signaling) overnight at 4°C. Detection was performed with a BM chemiluminescence Western blotting kit (Roche), and bands were visualized with a Kodak in vivo FX PRO system (Carestream Health). For semiquantitative analysis, bands were quantified and normalized to β-actin bands with Carestream spectral imaging software.

^{18}F-FLT and ^{18}F-FDG In Vitro Studies

HT29 cells (2×10^5/well) and MC26 cells (0.75×10^5/well) were plated in 24-well plates and allowed to attach by incubation overnight. The cells were incubated for 24 h with 0–10 mM MET (Sigma-Aldrich) dissolved in fresh culture medium. ^{18}F-FDG (370 kBq [10 μCi]/well) or ^{18}F-FLT (1,850 kBq [50 μCi]/well) was added directly to the culture medium, and the cells were incubated in a humidified incubator at 37°C with 5% CO_2 (60 min for ^{18}F-FDG and 2 h for ^{18}F-FLT). Next, the cells were placed on ice and washed 3 times with ice-cold PBS. The cells were trypsinized (trypsin–ethylenediaminetetraacetic acid; Invitrogen), transferred to counting tubes, and counted with a γ-counter (Wizard2; Perkin–Elmer). Radiotracer uptake was corrected for decay and cell count, and the percentage of retained activity/10^6 cells was reported.

Flow Cytometry, Cell Cycle, and Apoptosis Staining

The cells were plated and incubated as described earlier for ^{18}F-FLT and ^{18}F-FDG in vitro studies. After EdU (ethynyl

deoxyuridine) and annexin V–propidium iodide staining, the cells were kept on ice and protected from light until flow cytometry analysis with an LSRII apparatus (BD Pharmingen). Data were analyzed with preinstalled BD FACSDiva system software.

For determination of the percentage of S-phase cells in the cell population after MET treatment, a Click-iT EdU Alexa Fluor 647 kit (Invitrogen) was used. In brief, the cells were incubated with 10 μM EdU per well for 5 h in a humidified incubator at 37°C with 5% CO_2, washed with PBS, trypsinized, and collected by centrifugation (5 min; 1,200 rpm; room temperature [RT]). Next, the cells were resuspended (10^7 cells/mL) in 1% bovine serum albumin–PBS. The cell suspension (100 μL) was transferred to a fluorescence-activated cell sorting tube, washed with 3 mL of 1% bovine serum albumin–PBS, resuspended, and incubated with 100 μL of Click-iT fixative for 15 min at RT. Subsequently, the cells were washed, resuspended in 100 μL of Triton X-100–based permeabilization reagent, incubated for 15 min at RT, and washed again. Next, 0.5 mL of Click-iT reaction cocktail were added, and the cells were incubated for 30 min at RT (protected from light). The cells were washed and resuspended in 0.5 mL of 1% bovine serum albumin–PBS, 5 μL of ribonuclease A and 2 μL of propidium iodide were added to each tube, and the cells were incubated for 30 min at RT (protected from light) before flow cytometry analysis.

For determination of the percentage of apoptotic cells in the cell population after MET treatment, the cells were washed with PBS, trypsinized, and collected by centrifugation (5 min; 1,200 rpm; 4°C). Next, the cells were washed twice with ice-cold PBS and stained in accordance with the protocol used in an annexin V–fluorescein isothiocyanate apoptosis kit (BD Pharmingen). In brief, after resuspension of the cells (10^6/mL) in 1× binding buffer, 100 μL of the cell suspension were transferred to a fluorescence-activated cell sorting tube, 5 μL of annexin V–fluorescein isothiocyanate and 5 μL of propidium iodide were added, the contents of the tubes were mixed and incubated for 15 min at RT, 400 μL of 1× binding buffer were added, and flow cytometry analysis was performed.

^{18}F-FDG and ^{18}F-FLT In Vivo Studies with PET

All animal experiments were approved by the Institutional Animal Care Committee (Massachusetts General Hospital). HT29 cells were grown in cell culture medium until they were about 90% confluent. The cells were trypsinized, washed 3 times with PBS, collected by centrifugation (5 min; 1,200 rpm; RT), diluted to 50 × 10^6/mL in PBS, and kept on ice until injection.

Female nude mice (6–8 wk old, 2 groups of 5 each) were obtained from Charles River Laboratories International Inc. The tumors were established by subcutaneous injection of 20 μL (10^6 cells) of cell suspension. Imaging was performed 2–3 wk after injection and after the development of tumors of sufficient size (500 mm^3). Mouse anesthesia was maintained at a steady state with oxygen–1.5% isoflurane at 2 L/min. Calibrated doses of 18.5 MBq (500 μCi) of ^{18}F-FDG (first group) and 55.5 MBq (1,500 μCi) of ^{18}F-FLT (second group) were injected into mice via a catheter placed in the tail vein. At 1 h after injection in the ^{18}F-FDG group and 2 h after injection in the ^{18}F-FLT group, the mice were anesthetized again and imaged on an eXplore VISTA dual-ring small-animal PET scanner (GE Healthcare) for 15 min (2 bed positions). After imaging, the mice were treated for 24 h with MET (in PBS) at 500 mg/kg via intraperitoneal injection and imaged again with the same protocol after 24 h. This dose was selected for the in vivo experiments because previous studies demonstrated its biologic effects (*21*).

For assessment of potential changes in ^{18}F-FDG uptake in untreated animals over the same treatment period, an additional group of mice, which received no MET treatment, was imaged at time 0 and 24 h. Images were reconstructed with a 2-dimensional ordered-subset expectation maximization algorithm (4 iterations with scatter and random corrections) and GE system software. Three-dimensional regions of interest were manually defined on the tumors, and then mean standardized uptake values (SUVs) were calculated.

Statistical Analysis

Statistical analysis was performed with Prism software (version 5.00; GraphPad). Multiple-group analysis was performed with one-way ANOVA. The Tukey honestly significant difference post hoc test was applied for further analysis when statistical significance was observed on ANOVA. A paired *t* test was used for mean group comparison. Data are presented as mean ± SEM. *P* values of 0.05 or less were considered significant.

RESULTS

AMPK Activation

For confirmation of MET-mediated AMPK activation through AMPKα phosphorylation in colon cancer cell lines, Western blotting was performed with HT29 and MC26 cell lines after 24 h of treatment with 0–10 mM MET. As shown in Figure 2A, in both cell lines total AMPK levels remained essentially unchanged after treatment with various concentrations of MET. However, after gating of total AMPK levels to 100%, phosphorylated AMPK levels increased severalfold in a dose-dependent manner in both HT29 and MC26 cells (Fig. 2B).

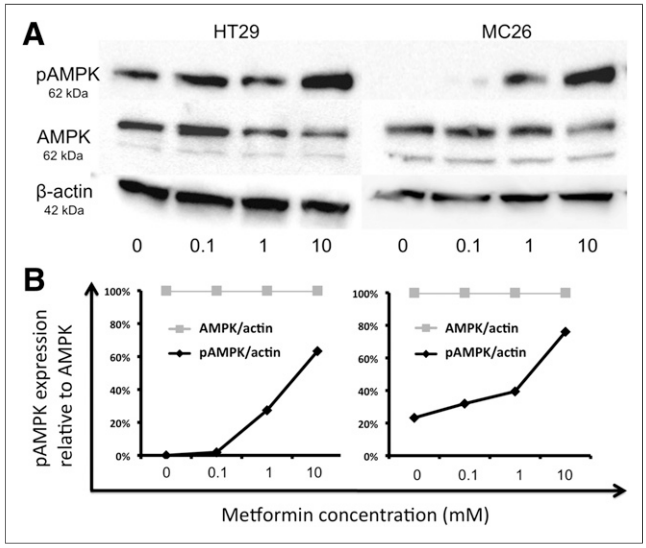

FIGURE 2. MET-mediated activation of AMPK. (A) Results of Western blotting for expression of AMPK, phosphorylated AMPK (pAMPK), and β-actin internal control in HT29 and MC26 cells after 24 h of MET treatment. (B) Semiquantitative analysis after gating of AMPK expression–to–actin expression ratio to 100% shows severalfold increases in phosphorylation and dose-dependent activation of AMPK in both cell lines.

Metabolic Changes

To evaluate changes in glucose uptake in tumor cells, we performed in vitro ^{18}F-FDG retention studies after incubation of cells with MET for 24 h. Dose-dependent increases in ^{18}F-FDG uptake were observed in both cell lines (Fig. 3). In HT29 cells, compared with the percentage of initial activity retention (0.13% ± 0.00%) in the control condition (no MET added), ^{18}F-FDG retention increased to 0.14% ± 0.00% ($P > 0.05$), 0.20% ± 0.01% ($P < 0.001$), and 0.49% ± 0.02% ($P < 0.001$) when the cells were treated for 24 h with 0.1, 1, and 10 mM MET, respectively. Similar results were observed for MC26 cells: ^{18}F-FDG uptake increased from 0.045% ± 0.005% (control) to 0.051% ± 0.001% with 0.1 mM MET ($P > 0.05$), 0.057% ± 0.002% with 1 mM MET ($P < 0.01$), and 0.099% ± 0.003% with 10 mM MET ($P < 0.001$).

Proliferation and Apoptosis Changes

The effect of MET on cellular proliferation was determined with in vitro ^{18}F-FLT retention studies and EdU flow cytometry analysis. As shown in Figure 4, ^{18}F-FLT uptake decreased in HT29 and MC26 cells with increasing MET concentrations. After 24 h, HT29 cells treated with 10 mM MET showed a lower level of ^{18}F-FLT uptake (2.63% ± 0.06% of initial added activity) ($P < 0.0001$) than cells in the control condition (4.46% ± 0.07%). Furthermore, the level of ^{18}F-FLT uptake was also lower when cells were exposed to 1 and 0.1 mM MET: 4.19% ± 0.14% ($P < 0.001$) and 3.02% ± 0.11% ($P < 0.001$), respectively.

These findings were further confirmed by EdU staining and flow cytometry, with which DNA proliferation was evaluated as a change in the percentage of S-phase cells. As shown in Figure 5, a marked decrease in the percentage of S-phase cells was found when HT29 cells were incubated with 10 mM MET—from 100.00% ± 1.09% (control) to 63.58% ± 1.86% ($P < 0.001$). No significant change in the percentage of S-phase cells was detected when HT29 cells were incubated with 1 mM MET (97.03% ± 3.82%) ($P > 0.05$).

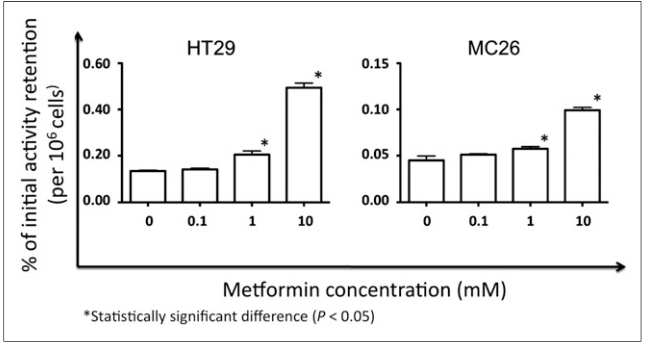

FIGURE 3. Alteration of ^{18}F-FDG uptake after MET treatment. MET treatment caused increased ^{18}F-FDG retention in both HT29 and MC26 cell lines. Results were corrected for decay and cell count and are presented as mean ± SEM ($n = 10$) percentage of initial activity absorbed/10^6 cells.

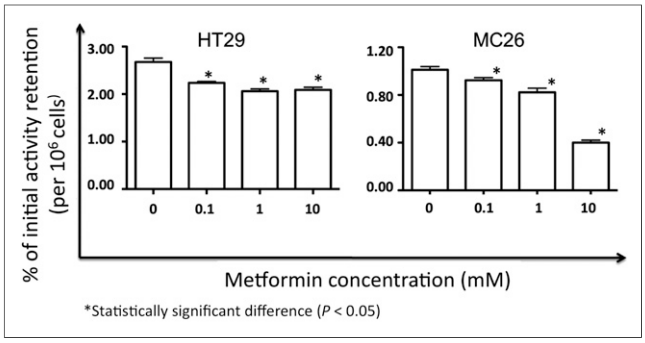

FIGURE 4. Effect of MET on ^{18}F-FLT retention. MET treatment decreased ^{18}F-FLT retention in both HT29 and MC26 cell lines. Results were corrected for decay and cell count and are presented as mean ± SEM ($n = 10$) percentage of initial activity absorbed/10^6 cells.

Similar results were obtained for MC26 cells. ^{18}F-FLT retention decreased from 1.01% ± 0.03% (control) to 0.92% ± 0.02% ($P < 0.01$), 0.82% ± 0.04% ($P < 0.001$), and 0.40% ± 0.02% ($P < 0.0001$) of initial activity when MC26 cells were incubated with 0.1, 1, and 10 mM MET, respectively (Fig. 4). In line with the ^{18}F-FLT changes, a decrease in the relative percentage of S-phase cells was found when MC26 cells were incubated with 10 mM MET for 24 h—from 100.00% ± 1.41% (control) to 66.10% ± 0.96% ($P < 0.001$) (Fig. 5). No significant change in the relative percentage of S-phase cells was detected when MC26 cells were incubated with 1 mM MET (98.95% ± 1.40%) ($P > 0.05$).

We noted similar decreases in the percentages of S-phase cells for both cell lines incubated with 1–10 mM MET, whereas ^{18}F-FLT uptake decreased in MC26 cells but not in HT29 cells incubated with 1–10 mM MET. These results

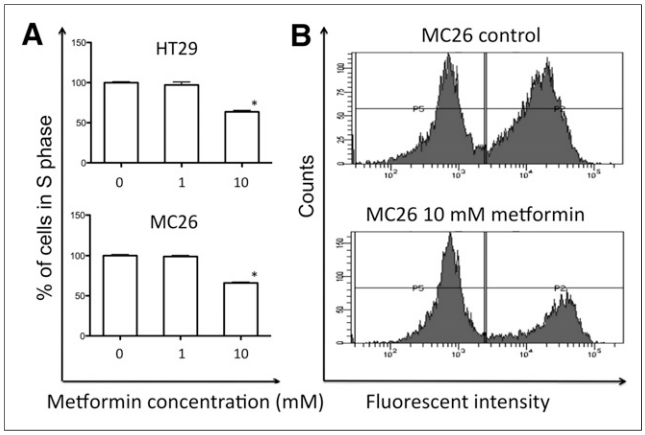

FIGURE 5. Effect of MET on proliferation. (A) Decreased relative percentages of cells in S phase of cell cycle (normalized to control at 100%) were observed in both cell lines (HT29 and MC26) after treatment with MET. Data are presented as mean ± SEM ($n = 3$). (B) Representative flow cytometry results from control and treatment groups of MC26 cells (10 mM MET for 24 h), with S-phase cells gated in P2 window.

TABLE 1
MET-Induced Apoptosis in HT29 and MC26 Cells After Incubation for 72 Hours

Cells	Condition	Mean ± SE no. of cells at MET concentration (mM) of: 0	0.1	1	10
HT29	Apoptosis	5.6 ± 0.36	5.47 ± 0.07	9.97 ± 0.52*	59.03 ± 0.85*
	Necrosis	1.63 ± 0.07	1.97 ± 0.57	4.23 ± 0.30*	8.27 ± 0.15*
MC26	Apoptosis	1.87 ± 0.09	1.83 ± 0.19	2.02 ± 0.15	10.93 ± 3.60†
	Necrosis	0.87 ± 0.12	0.73 ± 0.03	0.43 ± 0.03†	0.67 ± 0.07

*$P \leq 0.005$.
†$P \leq 0.05$.
For significance, MET incubation condition was compared with control condition (no MET added [0 mM]) ($n = 3$).

may reflect differences in the mechanisms of ^{18}F-FLT retention and EdU DNA incorporation.

Flow cytometry after staining for annexin–propidium iodide was performed to study the effect of MET on the rate of apoptosis in the colon cancer cell lines. No change in the apoptotic cell fraction was found 24 h after MET treatment (data not shown). The 72-h MET treatment resulted in a marked increase in the apoptotic cell fraction in both HT29 and MC26 cells (Table 1). After gating of the total cell population (live, apoptotic, and necrotic cells) to 100%, the percentage of apoptotic HT29 cells changed from 5.6% ± 0.362% when no MET was present to 5.47% ± 0.07% ($P > 0.05$), 9.97% ± 0.52% ($P < 0.01$), and 59.03% ± 0.85% ($P < 0.001$) in the presence of 0.1, 1, and 10 mM MET, respectively (Table 1). A significant increase in the percentage of apoptotic MC26 cells was observed when the cells were treated with 10 mM MET (10.93% ± 3.6% vs. 1.87% ± 0.09% [control]) ($P < 0.05$) but not lower concentrations of MET.

^{18}F-FDG and ^{18}F-FLT In Vivo Experiments

To confirm the in vitro results and extend the findings for translation to in vivo imaging, we performed experiments before and after MET treatment in nude mice bearing HT29 tumors. As shown in Figure 6, ^{18}F-FDG uptake in the tumors increased significantly after 24 h of MET treatment, whereas ^{18}F-FLT uptake decreased. After 24 h of MET treatment, measured mean tumor SUVs increased from 0.71 ± 0.03 to 1.29 ± 0.11 ($P < 0.05$) in the ^{18}F-FDG scans and decreased from 1.18 ± 0.05 to 0.89 ± 0.01 in the ^{18}F-FLT scans ($P < 0.05$). No significant changes in ^{18}F-FDG uptake were seen in the untreated control group tumors over the same time period, with SUVs of 1.24 ± 0.05 at time 0 and 1.15 ± 0.05 at 24 h ($P = 0.28$).

DISCUSSION

MET, an antidiabetes drug, has been used for decades for the treatment of type II diabetes and acts by decreasing glucose output from the liver and increasing glucose uptake in the peripheral tissues (*22*). There has been marked recent interest in oncologic applications of MET since the discovery of an epidemiologic correlation between a decreased incidence of cancer and the treatment of type II diabetes with MET, as highlighted in a recent metaanalysis (*23*). On the basis of the current available evidence, there is growing interest in using MET in combination with established therapeutic regimens; numerous oncology trials are currently recruiting patients to study the effects of MET on cancer incidence and progression (*3–6*). Moreover, MET serves as a prototypic agent in the expanding area of metabolic targeting for antineoplastic therapy (*24*).

MET is an activator of AMPK, which acts as the main cellular energy sensor. The effect on AMPK activity can be indirect, through the inhibition of adenosine triphosphate production in mitochondria, or direct, through increasing AMPK phosphorylation (*14,15*). The activation of AMPK

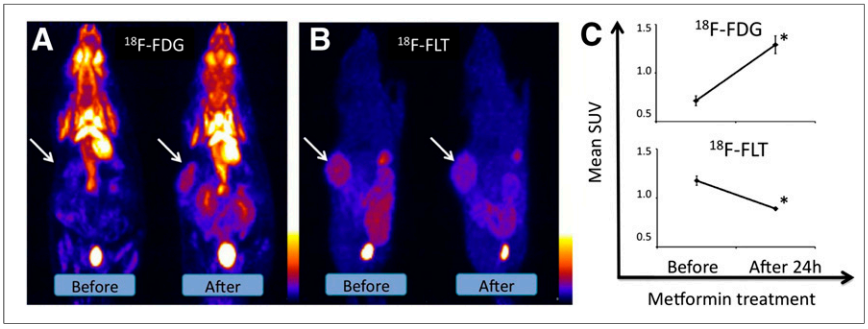

FIGURE 6. Increases in tumor ^{18}F-FDG uptake and decreases in ^{18}F-FLT uptake after MET therapy. PET images were acquired before (0 h) and after (24 h) MET therapy (500 mg/kg) in HT29 tumor–bearing animals. (A and B) Representative ^{18}F-FDG (A) and ^{18}F-FLT (B) PET scans before and after treatment. (C) SUVs before and after treatment (mean ± SEM; $n = 3$; imaged with both tracers). *Statistically significant difference ($P < 0.05$). White arrows indicate HT29 tumors.

downregulates many of the energy-consuming activities of cells, including protein, lipid, and nucleic acid synthesis, as well as proliferation; it upregulates pathways for energy production, such as glycolysis and fatty acid oxidation (*15,17*). As part of its function as a cellular energy sensor and regulator, AMPK—when phosphorylated—also induces Glut transporter externalization (*25,26*). We hypothesized that these AMPK-mediated changes in intracellular metabolic activity and in the Glut receptor level on the cell surface would directly increase tumor ^{18}F-FDG uptake. We further hypothesized that the same changes in the main energy sensor of cells would decrease ^{18}F-FLT uptake because of decreased nucleic acid synthesis and decreased proliferation. The data from the present study confirm our hypotheses and clearly demonstrate that MET—in a dose-dependent manner—suppresses the growth of cancer cell lines and decreases ^{18}F-FLT uptake both in vitro and in vivo but divergently increases ^{18}F-FDG uptake in both cell retention studies and PET studies. Our reported findings are in agreement with MET-induced AMPK activation through phosphorylation, which was confirmed by Western blotting, and its known effects on cellular metabolism.

To our knowledge, this is the first study reporting the consequences of MET treatment for radiotracer uptake modulation in tumors. To isolate the effects of MET, we selected monotherapy with various concentrations for the experiments to avoid any possible confounding effects from other chemotherapeutic drugs. However, in current oncology clinical trials, MET is being used in combination chemotherapy regimens (*27,28*). It is vital to understand how MET modulates the PET signal after therapy initiation; despite synergy, the MET-induced changes are opposite to the effects of other chemotherapies on tumor ^{18}F-FDG uptake. MET increases cellular ^{18}F-FDG uptake but, as the cells die from the effects of MET and other chemotherapies, ^{18}F-FDG uptake should eventually decrease. The resulting biphasic response on follow-up ^{18}F-FDG PET scans could confound the evaluation of therapeutic efficacy. Because of the initial increase in ^{18}F-FDG uptake, a patient might incorrectly be considered a nonresponder. Even on later scans, when the tumor bulk has partially decreased, a patient's response could be interpreted as inadequate because of the relative increase in ^{18}F-FDG uptake due to chronic AMPK activation in response to MET (*29*).

The confounding effects of MET on ^{18}F-FDG PET interpretation highlight the need to find a solution for similar situations when glucose modulators are being used incidentally or in combination treatments for cancer patients. Because both MET and many other chemotherapeutic drugs decrease tumor cell proliferation and increase cancer cell death and apoptosis, proliferation markers are an appropriate choice for imaging of the response of tumors in such situations. In the present study, we tested ^{18}F-FLT as a marker of proliferation to evaluate the effects of MET, given the well-established correlation between ^{18}F-FLT PET imaging and cell proliferation (*30,31*). Our results showed a strong correlation of ^{18}F-FLT uptake both in vitro and in vivo during PET scanning with cancer cell proliferation and apoptosis. These findings indicate that ^{18}F-FLT PET is appropriate for assessment of the chemotherapeutic response when glucose modulators are being used in combination chemotherapy regimens to avoid potential confounding effects on ^{18}F-FDG PET imaging. The use of ^{18}F-FLT instead of ^{18}F-FDG in such situations would also result in a monotonic response instead of the biphasic response of tumor ^{18}F-FDG uptake. Such concordant changes in ^{18}F-FLT PET will help speed optimization of the role of MET in combination regimens both preclinically and during clinical trials (*32*).

CONCLUSION

Our findings demonstrate that soon after the initiation of treatment, MET results in increased ^{18}F-FDG uptake, a corresponding increase in apoptosis, and decreased proliferation and ^{18}F-FLT uptake both in vitro and in vivo. ^{18}F-FLT uptake closely correlates with the tumor response to MET, whereas ^{18}F-FDG uptake does not. MET results in the divergent modulation of tumor cell growth and metabolism. Although experimental chemotherapy regimens were not evaluated in combination with MET, on the basis of the mechanisms elucidated here, ^{18}F-FLT may be a promising alternative to ^{18}F-FDG for the early noninvasive evaluation of standard and experimental chemotherapy regimens that include glucose modulators such as MET.

DISCLOSURE

The costs of publication of this article were defrayed in part by the payment of page charges. Therefore, and solely to indicate this fact, this article is hereby marked "advertisement" in accordance with 18 USC section 1734. This research was supported in part by National Institutes of Health grants U01CA143056, U01CA084301, and P50CA127003. No other potential conflict of interest relevant to this article was reported.

REFERENCES

1. Evans JM, Donnelly LA, Emslie-Smith AM, Alessi DR, Morris AD. Metformin and reduced risk of cancer in diabetic patients. *BMJ.* 2005;330:1304–1305.
2. Wright JL, Stanford JL. Metformin use and prostate cancer in Caucasian men: results from a population-based case-control study. *Cancer Causes Control.* 2009;20:1617–1622.
3. Lee JH, Kim TI, Jeon SM, Hong SP, Cheon JH, Kim WH. The effects of metformin on the survival of colorectal cancer patients with diabetes mellitus. *Int J Cancer.* 2012;131:752–759.
4. IRCCS San Raffaele. Combination chemotherapy with or without metformin hydrochloride in treating patients with metastatic pancreatic cancer (PACT-17). Available at: http://clinicaltrials.gov/ct2/show/NCT01167738. 2012. Accessed December 20, 2012.
5. Swiss Group for Clinical Cancer Research. Metformin hydrochloride as first-line therapy in treating patients with locally advanced or metastatic prostate cancer. Available at: http://clinicaltrials.gov/ct2/show/NCT01243385. 2012. Accessed December 20, 2012.
6. Ozmosis Research Inc. A trial of standard chemotherapy with metformin (vs placebo) in women with metastatic breast cancer. Available at: http://clinicaltrials.gov/ct2/show/NCT01310231. 2012. Accessed December 20, 2012.

7. Buzzai M, Jones RG, Amaravadi RK, et al. Systemic treatment with the antidiabetic drug metformin selectively impairs p53-deficient tumor cell growth. *Cancer Res.* 2007;67:6745–6752.
8. Green AS, Chapuis N, Maciel TT, et al. The LKB1/AMPK signaling pathway has tumor suppressor activity in acute myeloid leukemia through the repression of mTOR-dependent oncogenic mRNA translation. *Blood.* 2010;116:4262–4273.
9. Liu B, Fan Z, Edgerton SM, et al. Metformin induces unique biological and molecular responses in triple negative breast cancer cells. *Cell Cycle.* 2009;8:2031–2040.
10. Ben Sahra I, Laurent K, Loubat A, et al. The antidiabetic drug metformin exerts an antitumoral effect in vitro and in vivo through a decrease of cyclin D1 level. *Oncogene.* 2008;27:3576–3586.
11. Hirsch HA, Iliopoulos D, Tsichlis PN, Struhl K. Metformin selectively targets cancer stem cells, and acts together with chemotherapy to block tumor growth and prolong remission. *Cancer Res.* 2009;69:7507–7511.
12. Alimova IN, Liu B, Fan Z, et al. Metformin inhibits breast cancer cell growth, colony formation and induces cell cycle arrest in vitro. *Cell Cycle.* 2009;8:909–915.
13. Algire C, Amrein L, Zakikhani M, Panasci L, Pollak M. Metformin blocks the stimulative effect of a high-energy diet on colon carcinoma growth in vivo and is associated with reduced expression of fatty acid synthase. *Endocr Relat Cancer.* 2010;17:351–360.
14. El-Mir MY, Nogueira V, Fontaine E, Averet N, Rigoulet M, Leverve X. Dimethylbiguanide inhibits cell respiration via an indirect effect targeted on the respiratory chain complex I. *J Biol Chem.* 2000;275:223–228.
15. Hardie DG. AMP-activated/SNF1 protein kinases: conserved guardians of cellular energy. *Nat Rev Mol Cell Biol.* 2007;8:774–785.
16. Shackelford DB, Shaw RJ. The LKB1-AMPK pathway: metabolism and growth control in tumour suppression. *Nat Rev Cancer.* 2009;9:563–575.
17. Kahn BB, Alquier T, Carling D, Hardie DG. AMP-activated protein kinase: ancient energy gauge provides clues to modern understanding of metabolism. *Cell Metab.* 2005;1:15–25.
18. Gontier E, Fourme E, Wartski M, et al. High and typical ^{18}F-FDG bowel uptake in patients treated with metformin. *Eur J Nucl Med Mol Imaging.* 2008;35:95–99.
19. Ozülker T, Ozülker F, Mert M, Ozpacaci T. Clearance of the high intestinal ^{18}F-FDG uptake associated with metformin after stopping the drug. *Eur J Nucl Med Mol Imaging.* 2010;37:1011–1017.
20. Viljanen AP, Virtanen KA, Jarvisalo MJ, et al. Rosiglitazone treatment increases subcutaneous adipose tissue glucose uptake in parallel with perfusion in patients with type 2 diabetes: a double-blind, randomized study with metformin. *J Clin Endocrinol Metab.* 2005;90:6523–6528.
21. Zhang XF, Tan BK. Effects of an ethanolic extract of Gynura procumbens on serum glucose, cholesterol and triglyceride levels in normal and streptozotocin-induced diabetic rats. *Singapore Med J.* 2000;41:9–13.
22. Bodmer M, Meier C, Krahenbuhl S, Jick SS, Meier CR. Metformin, sulfonylureas, or other antidiabetes drugs and the risk of lactic acidosis or hypoglycemia: a nested case-control analysis. *Diabetes Care.* 2008;31:2086–2091.
23. Decensi A, Puntoni M, Goodwin P, et al. Metformin and cancer risk in diabetic patients: a systematic review and meta-analysis. *Cancer Prev Res (Phila).* 2010;3:1451–1461.
24. Vander Heiden MG. Targeting cancer metabolism: a therapeutic window opens. *Nat Rev Drug Discov.* 2011;10:671–684.
25. Winder WW, Hardie DG. Inactivation of acetyl-CoA carboxylase and activation of AMP-activated protein kinase in muscle during exercise. *Am J Physiol.* 1996;270:E299–E304.
26. Kudo N, Gillespie JG, Kung L, et al. Characterization of 5′AMP-activated protein kinase activity in the heart and its role in inhibiting acetyl-CoA carboxylase during reperfusion following ischemia. *Biochim Biophys Acta.* 1996;1301:67–75.
27. Martin-Castillo B, Vazquez-Martin A, Oliveras-Ferraros C, Menendez JA. Metformin and cancer: doses, mechanisms and the dandelion and hormetic phenomena. *Cell Cycle.* 2010;9:1057–1064.
28. Jalving M, Gietema JA, Lefrandt JD, et al. Metformin: taking away the candy for cancer? *Eur J Cancer.* 2010;46:2369–2380.
29. Li J, Benashski SE, Venna VR, McCullough LD. Effects of metformin in experimental stroke. *Stroke.* 2010;41:2645–2652.
30. Barthel H, Cleij MC, Collingridge DR, et al. 3′-deoxy-3′-[^{18}F]fluorothymidine as a new marker for monitoring tumor response to antiproliferative therapy in vivo with positron emission tomography. *Cancer Res.* 2003;63:3791–3798.
31. Pantaleo MA, Nannini M, Maleddu A, et al. Conventional and novel PET tracers for imaging in oncology in the era of molecular therapy. *Cancer Treat Rev.* 2008;34:103–121.
32. Jensen MM, Erichsen KD, Bjorkling F, et al. Early detection of response to experimental chemotherapeutic Top216 with [^{18}F]FLT and [^{18}F]FDG PET in human ovary cancer xenografts in mice. *PLoS One.* 2010;5:e12965.

The Journal of NUCLEAR MEDICINE

Metformin—an Adjunct Antineoplastic Therapy—Divergently Modulates Tumor Metabolism and Proliferation, Interfering with Early Response Prediction by ^{18}F-FDG PET Imaging

Peiman Habibollahi, Nynke S. van den Berg, Darshini Kuruppu, Massimo Loda and Umar Mahmood

J Nucl Med. 2013;54:252-258.
Doi: 10.2967/jnumed.112.107011

The Journal of Nuclear Medicine is published monthly.
SNMMI | Society of Nuclear Medicine and Molecular Imaging
1850 Samuel Morse Drive, Reston, VA 20190.
(Print ISSN: 0161-5505, Online ISSN: 2159-662X)

SNMMI SOCIETY OF NUCLEAR MEDICINE AND MOLECULAR IMAGING